Localized microstructural characterization of a dissimilar metal electron beam weld joint from an aerospace component

S. Jothi, Torsten Sebald, H.M. Davies, Eggert D. Reese, S.G.R. Brown

PII: S0264-1275(15)30697-3
DOI: doi: 10.1016/j.matdes.2015.10.119
Reference: JMADE 858

To appear in:

Received date: 25 July 2015
Revised date: 7 October 2015
Accepted date: 22 October 2015

Please cite this article as: S. Jothi, Torsten Sebald, H.M. Davies, Eggert D. Reese, S.G.R. Brown, Localized microstructural characterization of a dissimilar metal electron beam weld joint from an aerospace component, (2015), doi: 10.1016/j.matdes.2015.10.119

Localized microstructural characterization of a dissimilar metal electron beam weld joint from an aerospace component

***S. Jothi [1], Torsten Sebald [2], H.M.Davies[1], Eggert D. Reese [3], S. G. R. Brown [1]**

[1] College of Engineering, Swansea University, Singleton Park, Swansea SA2 8PP, UK
[2] Airbus Defence and Space, 81663 Munich, Germany
[3] Airbus Group Innovations, 81663 Munich, Germany
*S.Jothi@swansea.ac.uk

ABSTRACT

Hydrogen induced cold cracking (HICC) and hydrogen embrittlement (HE) are influenced by the microstructural evolution, residual plastic strain (i.e. local misorientation), recrystallization of grains and the resultant grain boundary characteristic distribution (GBCD) brought about by welding processes. HICC and HE are known to cause failures in aerospace components and it is vitally important to quantify the microstructural evolution, degree of residual plastic strain and determine the GBCD across dissimilar weld joints in order to assess the susceptibility of the weld joint to these phenomena. In this investigation a full a microstructural characterization study was carried out at various locations within and around a dissimilar weld joint of Pulse-plated Nickel (PP-Ni) and Inconel 718 (IN718), taken from an aerospace component. Areas examined included the base metals, weld fusion zone and heat affected zones on both sides of the weld joint, formed via electron beam welding. Scanning electron microscopy (SEM) in combination with electron backscatter diffraction (EBSD) was employed to measure the residual plastic strain, grain structure, grain size distribution, crystal orientation distribution, grain boundary misorientation distribution and GBCD of the dissimilar metal weld joint. Finally a metallurgical examination was carried out using SEM on the IN718 HAZ in order to investigate the secondary phase precipitation arising from the welding process. The results shows large variety of GBCD, crystallographic orientation distribution, local plastic strain distribution and grain size, shape and structure distribution across dissimilar weld joint. And these localized microstructural characterized data sets need to be carefully transferred using data-driven approach in order to develop predictive multiscale material modelling for hydrogen induced cracking and hydrogen embrittlement.

Keywords: Hydrogen induced cold cracking; residual plastic strain; Grain boundary characteristic distribution; dissimilar metal EB weld joint; Pulse plated Nickel, Inconel 718; SEM/EBSD;

1. Introduction

Hydrogen embrittlement (HE) and Hydrogen induced cold cracking (HICC) or cold cracking are costly problems in which structural degradation of the susceptible material can lead to catastrophic failure [1-10,12,17,47]. Several catastrophic failures have occurred in metallic material components due to hydrogen embrittlement and one such recent example is a long bolt in the 222-metre Leadenhall "cheese grater building" - the second tallest building in London, further details can be found elsewhere [11]. Another notable example is related to the San Fransciso-Oakland bay bridge. In March 2013, the shear key anchor safety rods catastrophically failed due to hydrogen embrittlement during the latter stages of construction. These 5m long 3-inch diameter threaded safety anchor rods, designed to protect the bridge in the event of seismic activity completely snapped into two parts. [1, 37-38].

HE, HICC and stress corrosion cracking (SCC) in the weld heat affected zone (HAZ), adjacent base metal and HAZ/base metal interfaces can be related to residual stresses present after electroplating and welding processes. Indeed, the presence of residual plastic strain within welded joints has caused concerns within the aerospace industry [12-14]. Hydrogen diffuses towards the tensile residual stress and residual plastic strain and segregates at these regions [12]. The base metal to HAZ interface between Nickel and Nickel based alloys has a complex microstructure. Grain recrystallization takes place in the HAZ under the thermal effect of the welding process. This can result in residual plastic strains and also changes in the grain structure and GBCD, ultimately leading to altered material properties and resistance to hydrogen embrittlement. A full understanding of these microstructural changes is of great scientific importance in order to determine the susceptibility to hydrogen embrittlement

within the HAZ/Base Metal (BM) interface and ultimately the structural integrity of the weldment and component. Scanning Electron Microscopy (SEM)/Electron Back scatter diffraction (EBSD) are an effective tool for measuring the microstructural features such as grain size, shape and distribution, crystal orientation, local misorientations (i.e. residual plastic strain) and GBCD [14-18].

The microstructural morphology such as crystal structure, grain size, grain shape, grain boundary characteristic distribution, crystal orientation, grain boundary misorientation, pores, atomic defects, triple junctions affects the bulk diffusion of hydrogen and distribution, segregation of hydrogen in metallic polycrystalline materials. Atomic hydrogen diffusion properties are different in grain interior, grain boundaries, triple junctions [5, 6, 8, 13, 24, 26-28, 30, 35, 38, 68]. And also different in different types of grain boundaries such as low angle grain boundary, high angle grain boundary, random grain boundaries, coincidence site lattice (CSL) and also it various depends on the connectivity of grain boundaries in triple junctions [54,56-58]. The microstructure features and microstructure inhomogeneity are significantly affects the distribution and segregation of atomic hydrogen leads to affects the mechanical properties, strength, ductility and structural integrity of the materials as well as hydrogen induced crack nucleation and crack propagation in the dissimilar weld joints of columnar and polycrystalline metallic materials. So it is important to understand microstructure features and characterize the weld joints microstructure.

In the present study, SEM and EBSD are utilised to investigate the microstructural evolution within dissimilar weld joints, the degree of residual plastic strain and Grain Boundary Character distribution (GBCD) across a weld joint, the heat affected zone and the base metals (BM) in this joint. A metallurgical examination was carried out in order

to understand the secondary phase precipitations within the HAZ in IN718 side using SEM. The specimen examined was taken from an actual aerospace component and is made of pulse -plated nickel (PP-Ni) and Inconel 718. The results are used to access the susceptibility of the part to hydrogen embrittlement.

2. Experimental methods:

2.1 *Materials and characterization procedure*:

A dissimilar metal joint, manufactured via electron beam (EB) welding and comprising PP-Ni and Inconel 718 was sectioned from an aerospace component and used for the material characterization within this study. The chemical composition of alloy 718 in weight percentage (wt%) is shown in the table1. The PP-Ni was manufactured using electroplating process were metal ions in the solution are moved to coat an electrode by an applied electric field under galvanostatic conditions. The normalized current density applied for pulse platting process to synthesis nickel as structural material was 150 and detail explanation about the manufacturing of PP-Ni can be found elsewhere [12,47]. The average concentration of impurity content in manufactured structural PP-Ni in parts per million (PPM) is shown in the table2 and hot gas extraction method was used to measure the average concentration of impurity content and its detail information can be found elsewhere [12, 47] .

Al	**B**	**C**	**Nb**	**Co**	**Cr**	**Cu**	**Fe**	**Mo**	**Ni**	**P**	**S**	**Si**	**Ti**	**Ta**
0.58	0.004	0.067	4.93	0.55	18.1	0.07	18.5	3.06	53.1	<0.005	<0.002	0.06	1.03	<0.05

Table1. Shows the chemical composition of alloy718 in weight percentage (wt%).

Hydrogen	oxygen	sulphur	carbon	Nitrogen
5	25	50	42	2

Table2. Shows the average concentration of impurity content in PP-Ni in PPM.

Figure 1 (a) shows a schematic diagram of the materials (PP-Ni/IN718) within the joint, (b) illustrates the position of the rolling direction (RD), transverse direction (TD), and normal direction (ND) of the specimen within the EBSD system and (c) is a macro-image of the dissimilar metal weld joint. EBSD micrographs were taken from the RD-TD plane so that the RD is vertical and the ND is horizontal. The section was prepared by mechanical grinding using P280 SiC grid paper for 3 minutes and mechanical polishing with 9 μm and 3 μm diamond suspensions for 5 minutes and 10 minutes respectively. Final polishing utilised 0.02 μm colloidal silica for 30 minutes to ensure a good surface finish. Electron backscatter diffraction analysis of the specimen was carried out using an Oxford Instruments channel 5 HKL system interfaced to a SEM. Analyses were performed at an accelerating voltage of 20 kV with a probe diameter (or) beam spot size of 7 nm. Several EBSD runs were carried out at various locations within the joint, namely, along the dissimilar weld joint root, above the weld root, within the In718 HAZ and base metal and within the PP-Ni HAZ and base metal. A step size of 0.2 μm and 4 μm was used in the EBSD analyses and more detailed information about post processing of the EBSD results and applying these data in multiscale modelling can be found elsewhere [19, 20].

In order to minimise the chance of any mis-indexing errors, nine Kikuchi bands were used for indexing. HKL-Tango software was used for post processing of the EBSD measured data in order to gather microstructural information such as grain boundary types, grain structure, grain size and crystallographic orientation distributions. In order to eliminate orientation noise, a 2° misorientation angle was used as a cut-off point. Misorientation angles of 15° or less were used to define low angle grain

boundaries (LAB). All the EBSD and SEM micrographs were taken in the RD-TD plane.

3. Results and discussion

The experimental results are divided into five sections as follows.

- In the first section, the grain structure and sizes of the dissimilar base metals and the microstructural evolution within the dissimilar weld joint have been studied.
- In the second section, the crystallographic misorientation distributions are mapped for the regions within and around the weld joint.
- The third section focusses on mapping the grain boundary characteristic distribution (GBCD) from the base metals and the highly deformed weld fusion zone (FZ), coarse grained heat affected zone (CGHAZ) and the less deformed fine grained hat affected zone (FGHAZ).
- In the fourth section, metallurgical examination has been carried out on the HAZ in In718.
- Finally, the local residual plastic strain concentration (i.e. local misorientation distribution) as the function of distance from the weld was measured.

3.1 Microstructure of the dissimilar base metals and microstructural evolution within dissimilar weld joints:

It has been reported by Oudriss and co-authors that change in the microstructural grain size affects the hydrogen permeation flux which is associated with the diffusion of hydrogen [5]. And the decreases in equiaxed polygonal structured grain size in pure nickel, increases the diffusivity of hydrogen at 300K. Jothi and co-authors reported that steady state hydrogen flux is smaller in larger grains which lead to decrease in the

diffusivity of hydrogen when grain size increases. And increase in the volume fraction of grain boundaries and triple junction also increases the effective diffusion of hydrogen in the bulk polycrystalline material based on multiscale modelling and experimental permeation test [6, 24, 26]. It was also supported by experimental investigation reported by Haris et al., Yao et al. and Tsuru et al. [23, 25, 27]. It was also reported that the presence of void in the polycrystalline material enhance the hydrogen trapping which may leads to hydrogen induced cold cracking due to the formation of methane and increase in the void also decreases the diffusivity due to increased trapping of hydrogen concentration [20, 30, 41]. Lattice defects [39, 63-64] and secondary phase distribution such as carbides in nickel based super alloy and steels act as hydrogen trapping sites [31-32, 62]. Hydrogen concentration in lattice defect and trap sites exceeds the critical level may initiates the hydrogen induced cracking. All these microstructural morphologies play a significant role in the phenomena such as hydrogen diffusion, distribution and segregation [33] and therefore affect hydrogen embrittlement and hydrogen induced cold cracking. The microstructural morphologies of a PP-Ni/In718 dissimilar metal weld joint has not, to the authors' knowledge, been studied. The objective of this section is to investigate the microstructural features of a dissimilar metal weld joint that occur using the electron beam welding process. The data and understanding gained through this experimental work will subsequently be transferred to support multiscale modelling of hydrogen diffusion and HE/HICC susceptibility as applicable to aerospace components. Details of the multiscale modelling work can be found elsewhere [41-42]. The dissimilar weld joint was characterized via EBSD analysis along the weld fusion zone, HAZs and the dissimilar base metals.

In recent years, EBSD has been widely used to characterize microstructure including grain area, grain size, crystal orientation, misorientations and grain shape [49-51]. Low angle grain boundaries (LABs) or sub-grain boundaries are those with a misorientation less than 15 degrees [49-52]. Misorientation angles are used to characterize grain boundary types e.g. low angle grain boundaries (LABs) and high angle grain boundaries (HABs) (i.e. θ>15°). HABs are further divided into coincident site lattice (CSL) and general or random grain boundaries (RGB) based on the atomic coincidence of neighbouring crystals at the grain boundary (GB) and the atomic density of defects [40, 50, 53]. The microstructures of the PP-Ni base metal, IN718 (i.e. the Nickel based superalloy Inconel 718), FZ and the HAZ were characterized and are shown in figure 2.

3.1.1 Microstructure of the base metals:

Figure 2 (a) shows the PP-Ni microstructural features such as grain structure, crystal orientation, and the corresponding colour–coded inverse pole figure (IPF). The total measured area was 17582μm^2 and the number of detected grains in this area was 38678 with distributions of grain diameter between 100nm to 3μm. Small and large columnar grains are seen, with an overall average grain size of 400nm (diameter) and average grain area of 1.76 μm^2. Columnar grains have grown in a direction parallel to the RD due to the pulsed electroplating process. Further information on the pulse plating technique can be found elsewhere [12]. Such a structure demonstrates that the pulse plating process has created a grain structure with a specific crystallographic orientation in this case orientation is along the <100>. Figure 2 (b) shows the same information for IN718 base metal. In this case, the average grain area was evaluated from 67 grains within an area of 9208512 μm^2. Very large columnar grains are found, with an average grain area of 54075μm^2. In this material, growth was predominantly in a direction

parallel to the TD with only a few "rolling direction" grain boundaries as shown in figure 2 (b). There is a marked difference in the grain area and grain size distribution between the PP-Ni and IN718 base materials both showing non-equiaxed structures.

3.1.2 Microstructural evolution in the heat affect zone (HAZ) on the PP-Ni side:

The microstructural evolution within the HAZ on the PP-Ni side was studied and the results are shown in figure 2 (c -e). Electron beam welding can significantly change the grain distribution, grain morphology and crystal orientations within the HAZ, depending on the weld heat source, heating rate and cooling rates. The grains observed within the PP-Ni HAZ are equiaxed. Within the HAZ, two different areas are clearly distinguishable, based on the grain size. The CGHAZ is formed of coarse grains and is defined as the coarse grain heat affected zone. Fine grains are found within FGHAZ which is defined as the fine grain heat affected zone FGHAZ. The CGHAZ is nearest to the FZ in figure 2 (c). Figure 2 (c) and (e) show the microstructural morphologies, crystal orientations and the crystal orientations of the PP-Ni side CGHAZ and FGHAZ in terms of Euler angles and IPF respectively. The colour contours for the Euler angles are shown in figure 2 (d). Due to the electron beam welding heat source the columnar grains in the PP-Ni base metal have undergone recrystallization and forming polygonal grains in CGHAZ and FGHAZ. The differences in grain sizes within CGHAZ and FGHAZ are due to the difference in the temperature distribution imparted by the heat source along the TD on the PP-Ni side during the welding process.

Coarse grains are observed up to a distance of approximately 350μm from the FZ along the TD and after that fine grains are detected up to a further 300μm from the FZ. It is therefore apparent that the welding process has caused recrystallization and grain growth to occur up to a distance of 650μm from the fusion zone. Temperatures imparted

during the welding process are higher in the CGHAZ than in the FGHAZ, consequently the CGHAZ region will take longer to cool than the FGHAZ region. The grain boundaries (GBs) within the PP-Ni CGHAZ can migrate more quickly when compared to the GBs in FGHAZ, due to the higher temperatures and slower cooling rates within this area during the welding thermal cycle.

3.1.3 Microstructural evolution within the heat affect zone of the IN718 and Fusion zone:

The microstructural evolution within the In718 HAZ and FZ was characterized via EBSD and the microstructure and measured grain orientations are shown in figure 2 (f). No major changes have occurred in the In718 as a result of the EB welding heat source.

There is little recrystallization and grain growth on the In718 side and only a very few recrystallized grains were observed in this region. The In718 possesses very large columnar coarse grains and the heat source is insufficient to allow any significant migration of the columnar grain boundaries. Only a few small grains are detected within the In718 HAZ and these smaller grains are secondary phase precipitations described in more detail in section 3.4. The FZ displays an inhomogeneous microstructure with both non-equiaxed columnar grains parallel to TD and equiaxed grains. The number of grains detected in the FZ was 701 with distributions of grain diameter ranging between 2μm to 100μm. Figure 3 (a) shows the statistical distribution of the grain size by diameter in the FZ calculated from 701 grains with a measured area of 480000μm^2.

Figure 3 (b) shows the statistical distribution of grain size by diameter within the PP-Ni. This distribution was calculated from an area of 17582μm^2 and the number grains detected was 38678. Figure 3 (c) shows the statistical distribution of grain size, by

diameter, from CGHAZ and FGHAZ within the PP-Ni side. The number of grains detected on the measured area of 49500 μm^2 in CGHAZ and FGHAZ are 1894 and 4545 respectively. The average grain size on PP-Ni, CGHAZ and FGHAZ are shown in table 3.

	CGHAZ	FGHAZ	PP-Ni
Average Grain Size	4.2μm	2.6μm	400nm
Measured Area	49500 μm^2	49500 μm^2	17582 μm^2
Number of Grains detected	1894	4545	38678

Table3. Shows the average grain size distributions measured by SEM/EBSD.

It has been reported that an increase in grain size will decreases the rate of hydrogen diffusion [5, 20, 24, and 41]. It is important to note that it may applicable for equiaxed polygonal structured grains and the rate of hydrogen diffusion in columnar grain structure are not explored very well. On this basis it would be expected that the effective diffusion of hydrogen in HAZ1 will be slower than in HAZ2. The grains detected in the PP-Ni are ultra-fine grains with an average grain size of 400nm, much smaller than the FG HAZ grains. Even though the measured area of the FZ was 27 times larger than the measured area of the PP-Ni region, the number of grains detected in the PP-Ni region was 55 times higher than the number grains detected in the FZ. Consequently the PP-Ni will have a much higher surface fraction of grain boundaries. For FCC nickel, an increase in the volume fraction of grain boundaries and a decrease in grain size have been reported to increase the rate of diffusion of hydrogen [5, 20, 24, and 41]. Again, based on the observed grain structures, the effective diffusion of hydrogen in PP-Ni would be expected to be much faster than the effective diffusion of hydrogen in CGHAZ and FGHAZ.

In addition to the difference in diffusivity of hydrogen between the FZ and IN718, there will also be a difference in hydrogen diffusivity between the PP-Ni base metal, HAZ1 and HAZ2. It has been previously reported that inequality or difference in the diffusion of metal ions results in the formation voids due to lattice drift which is related to the concept of Kirkendall effect [65-67]. Voids act as trapping sites for hydrogen. The segregation of atomic hydrogen in the trap sites forms hydrogen cluster and this hydrogen clusters are immobile and enhance the material degradation at the HAZ interface which may leads to HAZ interface fracture [8, 10]. This suggests that the gradient in hydrogen diffusivity may act as trap for atomic hydrogen at the CGHAZ-FGHAZ interface and also at the FGHAZ-PP-Ni base metal within the dissimilar metal weld joint. It has also been reported that a decrease in grain size in FCC nickel increases the geometrically necessary dislocation (GND) density and this GND can act as a "hydrogen trapping site" described by equation 1, [54, 55].

$$N_t^{GND} = \pi . r^2 . N_L . \rho_{GND} \quad (1)$$

Where, N_t^{GND} is the density of hydrogen trapping sites based on GND, ρ_{GND} is the GND density in m^{-2}, r is the effective distance from dislocation and N_L is the interstitial sites density in m^{-3}. Geometric necessary dislocation density is directly proportional to hydrogen trapping site density. So, an increase in geometric necessary dislocation density increases the density of hydrogen trapping sites. This clearly suggests that the PP-Ni has a higher amount of hydrogen trapping sites compared to IN718. In addition, weld residual stresses will also act as a trap for hydrogen within dissimilar metal weld joints. It is well known that the effective diffusion of atomic hydrogen in FCC polycrystalline nickel grain boundaries is two orders of magnitude faster when compared to the diffusion of atomic hydrogen in lattice sites [25-27]. Since a higher

volume fraction of grain boundaries is observed in the PP-Ni base metal compared to IN718, the PP-Ni may well act as a hydrogen trapping region within the dissimilar weld joint. In addition to this, an increased temperature will enhance the mobility of hydrogen atoms by increasing their jumping rates, possibly leading to an increase in hydrogen atom segregation at the grain boundaries. Segregated hydrogen along the grain boundaries increases the mobility of dislocations along the boundaries and reduces the ductility of the HAZ/PP-Ni interface.

3.2 GB Misorientation distributions within the dissimilar metal weld joint:

It has been previously reported that GB misorientations influence dislocations, micro-stress distributions and the atomic distribution and segregation of impurities such as hydrogen, oxygen and sulphur. They also play a prominent role in hydrogen, sulphur and oxygen induced cracking and embrittlement [8, 12, 43-47,].

In an attempt to understand this more fully statistical misorientation data has been extracted from the corresponding EBSD maps, figure 4 (a), and evaluated for the PP-Ni and IN718 grain boundaries. The misorientation distribution in PP-Ni shows that there is a distinct peak of misorientation angles less than 5°. Within the IN718 there is also a peak for misorientation angles less than 5° but here the peak is smaller, approximately one third of that shown for PP-Ni. Grain boundary misorientation has also been examined for the FZ, CGHAZ and FGHAZ, by extracting the statistical misorientation data from the corresponding EBSD measurements as plotted in figure 4 (a) and (b). Even in the FZ the distinct peak in GB misorientation angles less than 5° was observed similar to the PP-Ni. In order to assess the effect of the electron beam welding heat source on the development of the microstructural crystallographic misorientation distribution, the GB misorientation angles within the CGHAZ and FGHAZ were

calculated and plotted in figure 4 (b). Both CGHAZ and FGHAZ show two distinct peaks. The highest peak is observed at a GB misorientation angle of 60° and the second highest peak is observed at GB misorientation angles less than 5°. This shows that a large number of Σ3 grain boundaries were developed during the EB welding processing in both the CGHAZ and the FGHAZ.

From the HAZ1, HAZ2, FZ and PP-NI EBSD maps, the LABs and HABs GB misorientation partitions where calculated and plotted as shown in figure 4 (c). This shows that a low fraction of LABs are seen in FGHAZ and CGHAZ while a high fraction of LABs are detected in the FZ and the highest fraction of LABs are detected in the PP-Ni. This also shows that a high fraction of HABs are detected in HAZ1 and HAZ2 and fewer HABs are detected in the FZ. The lowest number of HABs is observed in the PP-Ni. It has been previously reported that an increase in HABs increases the likelihood of impurity atom segregation e.g. hydrogen, sulphur and oxygen, which can decrease the ductility and enhance brittleness at these GBs. This may lead to atomic impurity induced intergranular cracking and/or environmental induced intergranular cracking [4, 7-10, 19, 41, 43-46].

3.3 Grain boundary characteristic distribution of base metals and dissimilar weld joint:

The grain boundary characteristic distribution (GBCD) plays an essential role in several physical phenomena such as hydrogen embrittlement [7-10, 39], hydrogen diffusion [4-6], stress corrosion cracking [34-35] and fatigue [36]. Cold cracking in dissimilar weld joints is a major problem in manufacturing industries, especially in the aerospace sector, which needs to be better understood to reduce dissimilar weld joint

failures [12, 47]. The GBCD of PP-Ni/IN718 dissimilar weld joints have not been reported previously and thus provide motivation for the present work.

In this section, the GBCDs are categorised into three different types based on GB characteristics as described below.

- Low angle grain boundaries (LAB)
- Special coincident-site lattice with $\Sigma \leq 29$ (except $\Sigma 1$) are defined as Special grain boundaries (SCSL)
- General (or) Random (or) High angle grain boundaries (RGB)

The GBCDs of the PP-Ni, IN718, CGHAZ, FGHAZ and FZ were calculated from EBSD maps and the statistical distributions of GBCDs in terms of LAB, SCSL, RGB, $\Sigma 3$ are plotted in figure 5. The SCSL distributions in In718, PP-Ni, FZ, CGHAZ and FGHAZ were obtained from the analysis of several EBSD measurements as shown in figures 6 (a)-(e) with statistical distributions shown in figures 6 (f)–(j) respectively. It shows that very less number of grains is detected in PP-NI and on the other hand very high fractions of GBs are detected in PP-Ni. The fraction of RGBs observed in In718 and weld FZ are 81.5% and 83.67%. It also shows that FZ have highest fraction of RGB and FGHAZ have lowest fraction of RGB. There is no big difference in RGBs developed due to the effect of weld heat source between CGHAZ and FGHAZ. The EB weld heat source changes the microstructural grain boundary characteristic distribution in PP-Ni side HAZs. The microstructures in CGHAZ and FGHAZ in PP-Ni are recrystallized and developed a high fraction of SCSLs and a low fraction of RGBs in both CGHAZ and FGHAZ compared to base PP-Ni metal. The fraction of RGBs detected in PP-Ni base metal is 72.05%. The fraction of RGBs developed due to recrystallization in CGHAZ and FGHAZ are 62.65% and 62.52% respectively. The

amount of RGBs developed in PP-Ni side HAZs are reduced by approximately 10% when compared to the fraction of RGBs observed in PP-Ni base metal.

The fraction of SCSLs detected in CGHAZ and FGHAZ are 33.92% and 34.55% respectively. The fraction of SCSLs detected in PP-Ni base metal, FZ and In718 base metals are 8.9%, 4.07% and 9.36% respectively. The amount of SCSLs developed in PP-Ni side HAZs are increased by approximately 25% when compared to the fraction of SCSLs observed in PP-Ni base metal. This increase in SCSLs grain boundaries in CGHAZ and FGHAZ are mainly due to the increase in Σ3 type GBs. The fraction of Σ3 type grain boundaries in CGHAZ and FGHAZ are 27.56% and 24.5% respectively. The Σ3 type GBs are increased approximately by 22% in FGHAZ and 25% in CGHAZ when compared to base PP-Ni metal. Only, less than one percentage of Σ3 type grain boundaries detected in In718 base metal and FZ. The increase in the fraction of Σ3 type GB in CGHAZ and FGHAZ on the PP-Ni side would decrease the effective diffusion of hydrogen in these zones.

It has been reported that the diffusion of hydrogen in Σ3 type grain boundaries is slightly lower than the diffusion of hydrogen in bulk FCC polycrystalline nickel. The diffusivity of Σ3 type GBs is two orders of magnitude smaller than diffusivity of RGBs in FCC nickel [4, 25, 56-58]. It has been previously reported that enhanced diffusion of hydrogen are found in Σ5 and Σ9 type GBs. The diffusivities of Σ5 and Σ9 type grain boundaries are two orders of magnitude greater when compared to Σ3 and Σ11 type GBs in FCC nickel [4, 56-58]. Based on the difference in the diffusivity between different types of SCSL grain boundaries, it is further divided into three different families,

(i) The Σ3 and Σ11 type SCSL grain boundaries are called as slow diffusion SCSLs (i.e. SD-SCSL),

(ii) The Σ5, Σ7 and Σ9 type SCSL grain boundaries are called as fast diffusion SCSLs (i.e. FD-SCSL) and

(iii) All other SCSLs are called as random SCSLs (R-SCSL).

Figure 7 shows the calculated statistical distribution of SCSLs (i.e. Σ5, Σ7, Σ79, Σ11 and FD-CSL) in FGHAZ, CGHAZ and PP-Ni. The fraction of Σ5 type GB detected in CGHAZ, FGHAZ and PP-Ni base metal are 0.3%, 0.4% and 0.6% respectively. The fraction of Σ7 observed in CGHAZ, FGHAZ and PP-Ni base metal are 0.4%, 0.4% and 0.2% respectively. The fraction of Σ9 type GBs detected in CGHAZ, FGHAZ and PP-Ni base metal are 1.8%, 4.8% and 0.8% respectively. The fraction of Σ11 observed in CGHAZ, FGHAZ and PP-Ni base metal are 0.7%, 0.5% and 1.4% respectively. It shows fraction of Σ5 and Σ11 are higher in PP-Ni base metal when compared to PP-Ni side HAZs and on the other hand, the fraction of Σ7 and Σ9 are higher in PP-Ni side HAZs when compared to PP-Ni base metal. The fraction of FD-SCSL type family of SCSL grain boundaries are higher in FGHAZ, CGHAZ and PP-Ni base metal are 5.6%, 2.6% and 1.6% respectively. The effective grain boundary diffusion of hydrogen between CGHAZ, FGHAZ and PP-Ni base metal vary due to the different in the SCSL type grain boundary distribution. Increase in the fraction of FD-SCSL type SCSL grain boundaries increase the effective grain boundary diffusion of hydrogen in FGHAZ when compared to CGHAZ and PP-Ni base metal. It is well known that EB weld heat sources develop high degree of residual tensile stress in CGHAZ and FGHAZ. It was previously reported that the accumulation of tensile stress on grain boundaries increase the segregation of atomic hydrogen in these grain boundaries [8, 10, 20]. The increases in FD-SCSL in addition with tensile stresses developed due to weld heat sources increases the amount of hydrogen atom trapped at FGHAZ and CGHAZ. Increases in

the gradient of SCSL, RGBs in addition with increases in the gradient of weld residual stress, increases the possibility of hydrogen segregation in CGHAZ and FGHAZ. Increases in the segregation of hydrogen atom on CGHAZ and FGHAZ, decreases the ductility in this region which may lead to increase the possibility of hydrogen induced cracking susceptibility of dissimilar weld joints in CGHAZ and FGHAZ. On the other hand, the reader also needs to consider the other factors such as dislocations, pores/voids. And also the misfit between the coarse and fine grains on the interface between the CGHAZ, FGHAZ and PP-NI base metal due to welding cooling cycle.

There are few facts listed below that may have the possibility to segregates hydrogen atoms on the dissimilar weld joints which may enhances the material degradation leads to localized micro cold cracking.

Firstly, the pulse plating manufacturing technique will produce internal residual stresses in addition to the thermal residual stresses arising from welding which may also influence the distribution and segregation of hydrogen in the dissimilar weld joints and HAZs. Second, it should be noted that the base metal nickel material used in our study was manufactured using an electroplating process consisting of non-equiaxed columnar grains. This may influence the distribution of hydrogen of the dissimilar weld joints due to the fact that the diffusion of hydrogen in equiaxed polycrystalline microstructure and non-equiaxed columnar microstructure are different. Finally, due to the nature of the manufacturing technique (i.e. the applied pulse pattern in the electroplating process) hydrogen may be incorporated into the microstructure, with the amount dependent on the frequency, electrolyte and current applied during manufacturing. Thus in addition to microstructural features and manufacturing residual tensile stresses (arising from electroplating and welding), it appears that the introduction of hydrogen directly from

the manufacturing processes such as electroplating and welding could play a role in the susceptibility to hydrogen induced cracking in HAZs.

HAZs in PP-Ni, have been reported to be susceptible to weld cold cracking/HE [12, 47]. It has been previously reported that SCSL will enhance the resistivity to HE in nickel [7]. On the other hand, weld joints will develop thermal residual stress and it has been previously reported that residual tensile stress sites attract hydrogen atoms and accumulate high amount of hydrogens in these region. There is a possibility to reduces the susceptibility to hydrogen induced localized cold cracking by increasing the SCSL and reducing the residual stress based on grain boundary engineering (GBE) using systematic localized induction heat treatment near the dissimilar weld joints.

However, the EBSD investigation in this work indicates that relatively high fractions of SCSL are found in CGHAZ and FGHAZ on the PP-Ni side which can be still increased to high volume fractions using the proposed localized grain boundary engineering (GBE) on the dissimilar weld joints in order to decrease the susceptibility of cold cracking and increase the resistivity to hydrogen induced cold cracking.

3.4 Microstructure characterizations of weld metallurgy in the IN718 side of the HAZ in dissimilar weld joints:

The weld metallurgy in the HAZ on the In718 side near the top of the weldment was investigated using SEM and results are shown in figure 8. During weld solidification clusters of carbide phases were observed near the weld seam in the HAZ in In718 as shown in figure 8 (a). These precipitated secondary carbides are observed on intergranular gamma (γ) grain boundaries and in the intragranular γ matrix as shown in figure 8 (a), (b) and (c). Double layered secondary precipitates were also observed along the grain boundaries. Relatively low fractions of needle shaped secondary delta (δ)

phases were observed in γ GBs as shown in figure 8 (d). It has been previously reported that δ phase increases the susceptibility to HE in In718 [31] and hydrogen trapped at the δ phases may weaken the γ GBs interfaces where the δ phases are segregated [62]. Relatively high fractions of carbides are observed at the intragranular γ matrices in the HAZ in In718. Carbides can act as trapping sides for hydrogen so there may be an increased likelihood of atomic hydrogen segregation in the In718 HAZ in near the top of the weld where high fractions of carbides are observed. (This region would need to be treated carefully as a different zone when studying hydrogen diffusion and hydrogen embrittlement of dissimilar weld joints.

3.5 Evolution of the residual plastic strain on dissimilar weld joints BM of PP-Ni:

Kamaya and co-author reported the importance of local residual plastic strain arises due to the dislocation accumulation based on crystal orientation calculated using EBSD to evaluate the SCC [16, 21, 22]. According to the knowledge of authors there is very little study or no study has been carried out to calculated local residual plastic strain due to the dislocation accumulation developed by EB welding on the PP-Ni/In718 dissimilar weld joints. This motivates the authors to investigate the local residual plastic strain on dissimilar weldment. The local residual plastic strain distributions in the microstructures of PP-Ni, In718, weld FZ, HAZ2 and HAZ1 are shown in figure 9 (a) to (e) respectively. The local misorientation maps (defined as the average misorientation of a point and its eight nearest neighbours) have been used to describe the residual plastic strain concentration at grain lattices and grain boundaries [21-24, 9, 61, 70]. As illustrated in figure 9 (a), the PP-Ni displayed a high degree of residual plastic strain concentration, due to the presence of a large number of ultra-fine columnar grains. The effect of electro-plating parameters plays a role in this local residual plastic strain. As

illustrated in figure 9 (b), In718 shows low degree of residual plastic strain concentration. This is due to the presence of small misorientation gradient with in the grains and less orientation gradient between neighbouring grains. The presence of low degree of residual plastic strain concentration in In718 is also as result of small misorientation differences between neighbouring points in grains. Figure 9 (c) illustrates the high degree of localized residual plastic strain concentration in the FZ even though large columnar grains are observed in these regions. Red colour shows the high degree of localized plastic strain and blue colour shows the low degree of localized residual plastic strain. The localized plastic residual strain within two different grains (i.e. grain1 and grain2) in FZ is plotted which shows high degree of localized plastic strains in FZ when compared to HAZs and In718. High degree of residual plastic strain concentration generated in FZ are due to large orientation differences between neighbouring points with in individual grains that occurs as a result of dislocation accumulation introduced by heterogeneous plastic deformation during welding heat sources. This indicates that the EB welding process caused a high degree of local residual plastic strain concentration within grains and grain boundaries. The residual thermal stresses caused by the weld heat source develop a high atomic misfit on grain boundaries due to anisotropic crystallographic orientation leading to the observed high degree of local misorientations at grain boundaries. Considering the HAZs figures 9 (d) and (e), a relatively high degree of residual plastic strain concentration compared to In718 is observed. This is lower, however than that seen for the PP-Ni and FZ.

This lower residual plastic strain concentration corresponds to the lower welding heat input at these areas compared to FZ. The FGHAZ shows a higher residual plastic

strain concentration than the CGHAZ and this may be due to the presence of a higher fraction of grain boundaries within in FGHAZ.

Figures 10 (a)-(e) show the calculated local misorientations plotted as a function of distance along TD in PP-Ni, In718, CGHAZ, FGHAZ and FZ respectively. Peaks of local misorientations are apparent at grain boundaries as expected. A large number of peaks are observed in the PP-Ni (i.e. up to a distance of 120μm), on the other hand very few numbers of peaks was observed on In718 base metal (i.e. in the 3mm). Figure 10 (c), (d) and (e) illustrate that fewer misorientations peaks are seen within the CGHAZ when compared to FGHAZ. The fusion zone displays significantly fewer misorientation peaks than either the FGHAZ or the CGHAZ. It has been reported previously that local misorientations are proportional to geometric necessary dislocation density, equation 2, and GND densities may act as atomic hydrogen trapping sites in FCC nickels as previously described in equation 1 [5, 54, 69].

$$\rho_{GND}^{a} = \frac{1}{2d}\sum_{j=1}^{m_{gb}}\frac{1}{s_j} = \frac{1}{bd}\sum_{j=1}^{m_{gb}} sin\left(\frac{\theta_j}{2}\right).f_j \qquad (2)$$

Where $\rho_{GND}^{a}$the average GND density (m-2), b is is Burgers vector, d is grain size, m_{GB} is number of GBs studied, s_j is the distance between two dislocations in a GB misorientation of θ_j where from dislocation theory $s = \frac{b}{2}\sin\left(\frac{\theta}{2}\right)$ [69], θ_j is misorientation angle and f_j is the fraction of misorientation angle. Thus an increase in misorientation angle increases the GND density which increases the number of hydrogen trapping sites. Thus FGHAZ, FZ and PP-Ni have a greater tendency to hydrogen trapping compared to CGHAZ and IN718 corresponding to the increased amount of local residual strain concentration.

Huge amount of data and data sets are collected in this localized microstructural characterization of dissimilar weld joints of aerospace component which need to be

handled carefully and transferred in order to study and develop predictive multiscale material models for hydrogen embrittlement and hydrogen induced cracking. In addition to this huge amount of data was collected previously through EU FP7 "MultiHy" project in order to understand the hydrogen diffusion, stress assist hydrogen distribution and hydrogen induced cracking in aerospace application and also in automotive, renewable energy applications using atomic, meso-scale, microstructural, macro-scale modelling and experimentation [6, 8, 10, 12, 13, 19, 20 ,24, 26, 30, 41, 42, 47, 56, 57]. All these data need to be properly stored and systematically studied in order to understand and develop predictive model for hydrogen embrittlement using data-driven approach.

4. Conclusions

Progress has been made in the understanding of the microstructural evolution, grain boundary character distribution and residual plastic strain distributions within a dissimilar metal weld joint and how they can be related to hydrogen diffusion and embrittlement. SEM/EBSD analysis has been used to evaluate the microstructural features of the dissimilar base metals (PP-Ni and In718) and also the microstructural evolution that occurs within the weld fusion zone, and different HAZ regions within the In718 and PP-Ni. The analysis has demonstrated that the Electron beam weld heat source affects the grain morphology, grain size distribution, GBCD and residual plastic strain concentrations in dissimilar weld joints. The fraction of HABs, LABs, CSL boundaries and residual plastic strain concentrations in dissimilar weld joints have been quantified?. The following conclusions have been drawn from the investigation.

- Non-equiaxed, very coarse, columnar grains are found within the In718 base metal compared to non-equiaxed, fine, columnar grains within the PP-Ni base metal.
- A large amount of recrystallization was observed in the PP-Ni side HAZ. Much less recrystallization had occurred within the HAZ on the In718 side.
- Recrystallized grains take the form of equiaxed polygonal grains in both the CGHAZ and the FGHAZ on PP-Ni side.
- Grain size distributions vary greatly across the joint. The detected grain sizes range from >1mm in the In718 to less than 400nm in the PP-Ni.
- A high fraction of HABs were observed in both the FGHAZ and CGHAZ areas on the PP-Ni side. The proportion of HABs in the HAZ has increased by approximately 45% when compared to HABs within the base metal.
- The proportion of LABs in the PP-Ni side HAZ has decreased by approximately 16% when compared to LABs in PP-Ni base metal.
- An increase in the fraction of HABs and decrease in the fraction of LABs in PP-Ni side HAZs can lead to an increase in the effective grain boundary diffusion of hydrogen in these regions.
- An increase in the fraction of FD-SCSL type grain boundaries within the FGHAZ and CGHAZ increases the effective diffusion of hydrogen.
- High volume fractions of residual plastic strains are detected within the PP-Ni base metal, less residual plastic strain has been observed within In718 base metal. An increase in residual plastic strain will increase the number of hydrogen trapping sites.

- High fractions of local misorientations are detected in the weld FZ, the HAZs and the PP-Ni base metal when compared to In718. Increases in local misorientation increases the fraction of GND.
- Metallographic investigation using SEM in the HAZ in In718 shows secondary precipitates on intergranular and intergranular γ matrix. Precipitation of carbide secondary phases has been detected in In718 side HAZ.

The present study on microstructural characterization provides much of the data needed for the challenging future work of understanding and quantifying hydrogen diffusion, hydrogen induced cold cracking and hydrogen embrittlement in aerospace component dissimilar weld joints. The present work also highlights the multiscale nature of the problems which lead to hydrogen induced failure on aerospace component dissimilar weld joint. To properly study the hydrogen diffusion, hydrogen embrittlement in PP-Ni/In718 dissimilar weld joints in aerospace components, either via multiscale modelling or experimentation using data-driven approach, all of these localized microstructural characterizations would need to be carefully considered and taken into account based on data-driven approach. In addition to that the authors also propose the concept of grain boundary engineering using localized induction heat treatment on the dissimilar weld joints to enhance the SCSL in order to enhance the resistivity to hydrogen induced cold cracking.

Acknowledgements

This work was supported by EU 7th Framework program through the project MultiHy (Multiscale Modelling of Hydrogen Embrittlement) under Project No. 263335. The

author S. Jothi also gratefully acknowledges the assistance of the MACH1 Laboratories at Swansea University.

References:

[1] http://www.fastenerandfixing.com/fastenerandfixing/News/Entries/2015/1/22_Continued_controversy_over_Bay_Bridge_embrittlement_failures.html, published on 22nd Jan 2015

[2] P. Hicks, C. Alstetter, Metall. Trans. A 1992; 23A:237-249.

[3] J. Song, W.A. Curtin, Nature Mat. 2013; 112:145-151.

[4] B.Ladna, H.K. Birnbaum, Acta Metall. 1987; 35:1775-1778.

[5] A.Oudriss, J.Creus, J.Bouhattate, E. Conforto, C. Berziou, C. Savall, X. Feaugas, Acta Materialia 2012;60:6814-6828.

[6] S. Jothi, N.Winzer, T.N. Croft, S.G.R. Brown, J. Alloys and Compounds 2015; In Press, http://dx.doi.org/10.1016/j.jallcom.2014.12.247

[7] S.Bechtle, M.Kumar, B.P. Somerday, M.E. Launey, R.O.Ritchie, Acta Materialia 2009; 57:4148-4157.

[8] S. Jothi, T.N. Croft, S.G.R. Brown., Int. J Hydrogen energy 2014; 39:20671-20688.

[9] M. Seita, J.P.Hanson, S. Gradecak, M.J.Demkowicz, Nature Communications 2015; 6: doi: 10.1038/ncomms7164.

[10] S. Jothi, T.N. Croft, S.G.R. Brown, Journal of Alloys and Compounds 2014; In press, doi:10.1016/j.jallcom.2014.12.073.

[11] "The Guardian" http://www.theguardian.com/business/2015/jan/14/cheesegrater-leadenhall-building-bolt-city-london, published on 14th Jan 2015.

[12] E.D. Reese, W.V.Bestenbostel, T.Sebald, G.ParoNis, D.Vanelli and Y.Muller, JOM 2014; 66:1368-1376.

[13] S. Jothi, T.N. Croft, L. Wright, A. Turnbull, S.G.R. Brown, Multi-phase modelling of intergranular hydrogen segregation/trapping for hydrogen embrittlement, International journal of hydrogen energy 2015; In Press.

[14] A.J.Wilkinson, P.B.Hirsch, Micron 1997; 28:279-308.

[15] A.J.Wilkinson, Scripta Mater. 2001; 44:2379-2385.

[16] M.Kamaya, A.J.Wilkinson, J.M.Titchmarsh, Nuclear Engineering and Design 2005; 235:713-725.

[17] S. Kobayashi, T. Maruyama, S. Tsurekawa, T. Watanabe, Acta Materialia 2012; 60:6200-6212.

[18] V. Randle, H. Davies, I. Cross, Current Opinion in Solid State and Materials Science 2001;5:3-8.

[19] S.Jothi, S.V.Merzlikin, J.Andersson, T.N.Croft, S.G.R.Brown, An investigation of micro-mechanisms in hydrogen induced cracking in Nickel based superalloy 718; (In Review),

[20] S.Jothi, Multiscale modelling and experimentation of hydrogen embrittlement in aerospace materials, PhD Thesis 2015.

[21] M. Kamaya, A.J. Wilkinson, J.M. Titchmarsh, Acta Materialia 2006; 54:539-548.

[22] M. Kamaya, A.J. Wilkinson, J.M. Titchmarsh, Nuclear Engineering and Design 2005; 235:713-725.

[23] T.M. Harris, L.M. Latanision, Metall Trans A 1991; 22A:351

[24] S. Jothi, T.N. Croft, S.G.R. Brown, E.A. de Souza Neto, Composite Structures 2014; 108:555-564.

[25] T. Tsuru, R.M. Latanision, Scripta Metall 1982; 16:575-578.

[26] S. Jothi, T.N. Croft, S.G.R. Brown, Int. J Hydrogen energy 2015; 40:2882-2889.

[27] J. Yao, J.R. Cahoon, Acta Metall Mater 1991; 39:119

[28] L. Hu, R. Huo, J. Zho, Y. Wang, S. Zhang, J Nanopart Res 2012; 14:667.

[29] I.M. Mikhailovski, V.B. Rabukhin, O.A. Velikodnaya, Phys status Solidi A 1991; 125:K65.

[30] S. Jothi, T.N. Croft, S.G.R. Brown, Composites Part B: Engineering 2015; 75:104-118.

[31] L. Liu, C. Lu, W. Ding, A. Hirose, K.F. Kobayashi, J. Mater. Sci. Technol. 2005; 21:256-260.

[32] M, Au, Journal of Alloys and Compounds 1999; 293-295:317-323.

[33] R.M. Latanision, H. Opperhauser Jr., Metall Trans A 1973; 5:483-492.

[34] M.A. Arafin, J.A. Szpunar, Corrosion Science 2009; 51:119-128.

[35] G. Palumbo, P.J. King, K.T. Aust, U. Erb, P.C. Lichtenberger, Scripta Metallurgica et Materialia 1991; 25:1775-1780.

[36] S.Kobayashi, T.Inomata, H.Kobayashi, S.Tsurekawa, T.Watanabe, J Mater Sci 2008; 43:3792-3799.

[37] http://www.baybridgeinfo.org/rods, (2015).

[38] Toll bridge program oversight committee "Report on the A354 Grade BD high-Strength Steel Rods on the New East Span of the San-Francisco-Oakland Bay Bridge with Findings and Decisions", July 8, 2013.

[39] T. Doshida, M. Nakamura, H. Saito, T. Sawada, K. Takai, Acta Materialia 2013; 20:7755-7766.

[40] V. Randle, The Role of the Coincidence Site Lattice in Grain Boundary Engineering 1996,

[41] S. Jothi, T.N. Croft, S.G.R. Brown, "European Union FP7 Multi-Scale Modelling Hydrogen Embrittlement - MultiHy", Swansea University reports (2014, 2015).

[42] S. Jothi, T.Sebald, T.N. Croft, E.D. Reese, S.G.R. Brown, "Multiscale modelling and experimentation: Anisotropic diffusion of hydrogen on pulse plated Nickel"(2015 In preparation).

[43] H.Chen, R.K. Kalia, E. Kaxiras, G. Lu, A.Nakano, K. Nomura, A.C.T. van Duin, P. Vashishta and Z. Yuan, Embrittlement of Metal by Solute Segregation-induced Amorphization, Phys. Rev. Lett. 2010; 104:155502.

[44] R.M. Krishnan, B.R. Nijhawan, Failures of Metals in Sulphur & Sulphur Bearing Media, Symposiu on Industrial Failure of Engineering Metals & Alloys, Feb 5-7 Jamshedpur 1953;

[45] H. Uetsuka, T. Furuta and S. Kawasaki, Embritlement of Zircaloy-4 due to oxidation in Environment of Stagnant Steam, Journal of Nuclear Science and Technology 1982;19:158-165.

[46] H. Dugdale, D.E.J. Armstrong, E. Tarleton, S.G. Roberts, S.Lozano-Perez, How Oxidized grain boundaries fail, Acta Materialia 2013; 61:4707-4713.

[47] E.D. Reese, T. Sebald, European Union FP7 Multi-Scale Modelling of Hydrogen Embrittlement – MultiHy project", AIRBUS reports (2013, 2014 and 2015).

[48] P.R. Cantwell, M. Tang, S.J. Dilon, J. Luo, G.S. Rohrer and M.P. Harmer, Grain boundary Complexions, Acta Materialia 2014;62:1-48.

[49] A. Bastos, S. Zaefferer, D. Raabe, C. Schuh, Acta Mater. 2006; 54:2451.

[50] C.Savall, A. Godon, J. Creus, X. Feaugas, Surface & Coating Technology 2012;206:4394-4402.

[51] F.J.Humphreys, J. Mater. Sci. 2001; 36:3833.

[52] F. Dalla Torre, A. Gazder, C. Gu, C. Davies, E. Pereloma, Metall. Mater. Trans. A 2007; 38A:1080.

[53] T.Ungar, J. Mater. Sci. 2007; 42:1584.

[54] A. Oudriss, J. Creus, J. Bouhattate, C. Savall, B. Peraudeau and X. Feaugas, Scripta Materialia 2012; 66:37-40.

[55] Y. Mine, Z. Horita, Y. Murakami, Acta Mater. 2009; 58:649-657.

[56] D.D.Stefano, M.Mrovec, C.Elasasser, First principles investigation of hydrogen trapping and diffusion at grain boundaries in Nickel, Acta Materialia (2015) (submitted).

[57] D.D.Stefano,M.Mrovec, C.Elasasser, MultiHy Project report IWM (2014).

[58] M.L. Martin, B.P. Somerday, R.O. Ritchie, P. Sofronis, I.M. Robertson, Acta Materialia 2012; 60:2739-2745.

[59] J. Hou, Q.J. Peng, Z.P. Lu, T. Shoji, J.Q. Wang, E.-H. Han, W. Ke, Corrosion Science 2011; 53:1137-1142.

[60] A. Saez-Maderuelo, L. Castro, G. de Diego, Journal of Nuclear Materials 2011; 416:75-79.

[61] J. Hou, Q. Peng, Y. Takeda, J. Kuniya, T. Shoji, Corrosion Science 2010; 52:3949-3954.

[62] L.FourNier, D. Delafosse, T. Magin, Mater. Sci. Engng A 1999; 269A:111.

[63] T. Doshida, K. Takai, Acta Materialia 2014; 79:93-107.

[64] K. Takai, H.Shoda, H. Suzuki, M. Nagumo, Acta Materialia 2008; 18:5158-5167.

[65] E.O. Kiekendall, Trans. Am. Inst. Min., Metall. Pet. Eng. 1942; 147:104.

[66] L. Klinger, E. Rabkin, Acta Materialia 2011; 59:1389-1399.

[67] A.D. Smigelskas and E.O. Kirkendell, Trans. Am. Inst. Min., Metall. Pet. Eng. 1947; 171:130.

[68] Y. Chen, C.A. Schuh, J. Appl. Phys. 2007; 101:063524.

[69] J.F.Nye, *Acta Metall*. 1 (1953) 153-162.

[70] S.I. Wright, M.M. Nowell, D.P. Field, A review of strain analysis using electron backscatter diffraction, Microsc. Microanal. 17 (2011) 316-329.

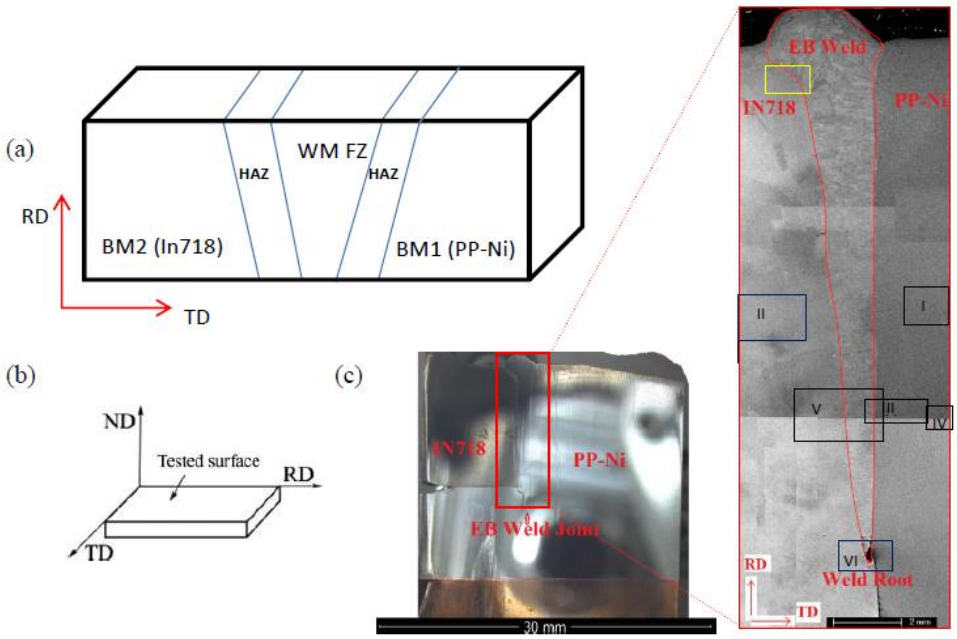

Figure 1 (a) Schematic diagram of dissimilar metal electron beam weld joint, weldment (WM), fusion zone (FZ), Base metals (BMs) (i.e. PP-Ni and IN718) and Heat Affected Zones (HAZs) (b) EBSD specimen orientation. (c) 'Nail pattern' dissimilar electron beam (EB) weld joint. Note: Black boxes and Roman numerals show the positions at which EBSD investigations were performed, the yellow box shows the region analysed using SEM.

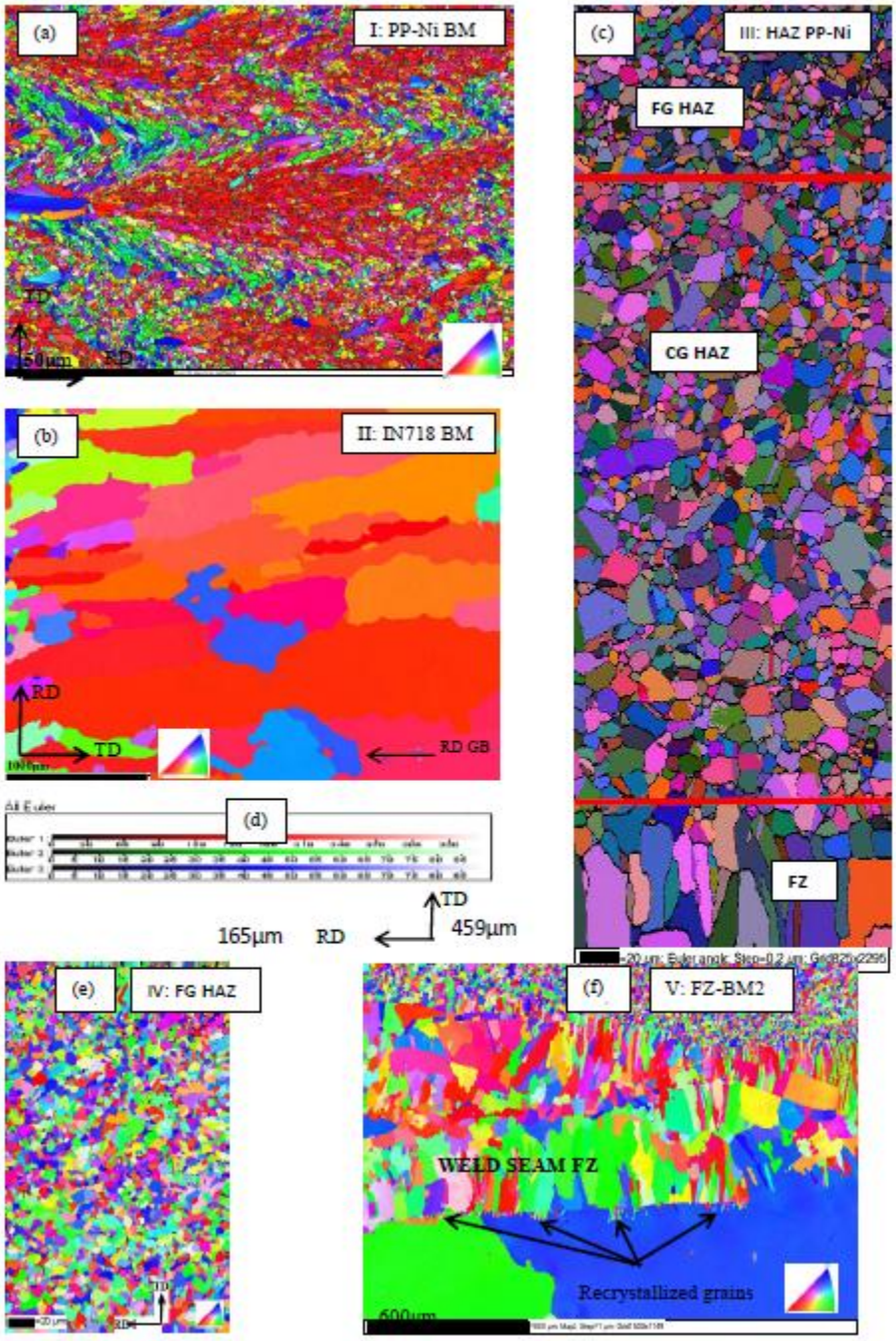

Figure 2 EBSD results for (a) PP-Ni base metal (b) IN718 base metal, (c) crystal orientations in Euler angles for the fusion zone (FZ) and heat affected zone (HAZ) along the PP-Ni side of the dissimilar weld joint. (d) Euler angle colour contour. (e) Crystal orientations in fusion zone (FZ) and heat affected zone (HAZ) along the IN718 side of the dissimilar weld joint. (f) Misorientation distribution between PP-Ni, IN718 and weld FZ. Note: Black scale bars are (a) 50µm and (b) 1000µm (c) 20µm (e) 600µm. (Note: Readers are referred to the web version on this article for the interpretation of the reference to colour in the figure legend. (Roman numerals indicate the position of EBSD measurements c.f. figure 1(c).)

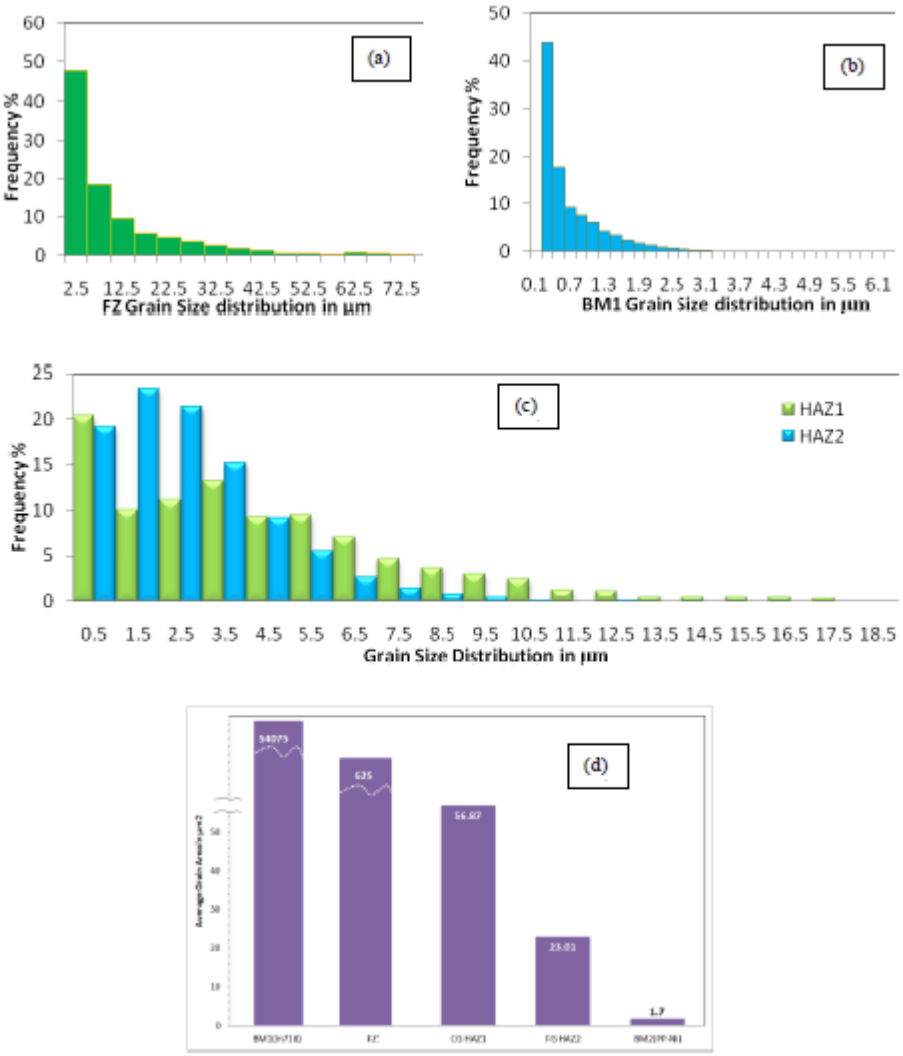

Figure 3 Statistical distribution of grain size distribution of (a) FZ, (b) PP-Ni, and (c) HAZ on the PP-Ni side of the weld. (d) Average grain area in the PP-Ni/IN718 dissimilar metal weld joint.

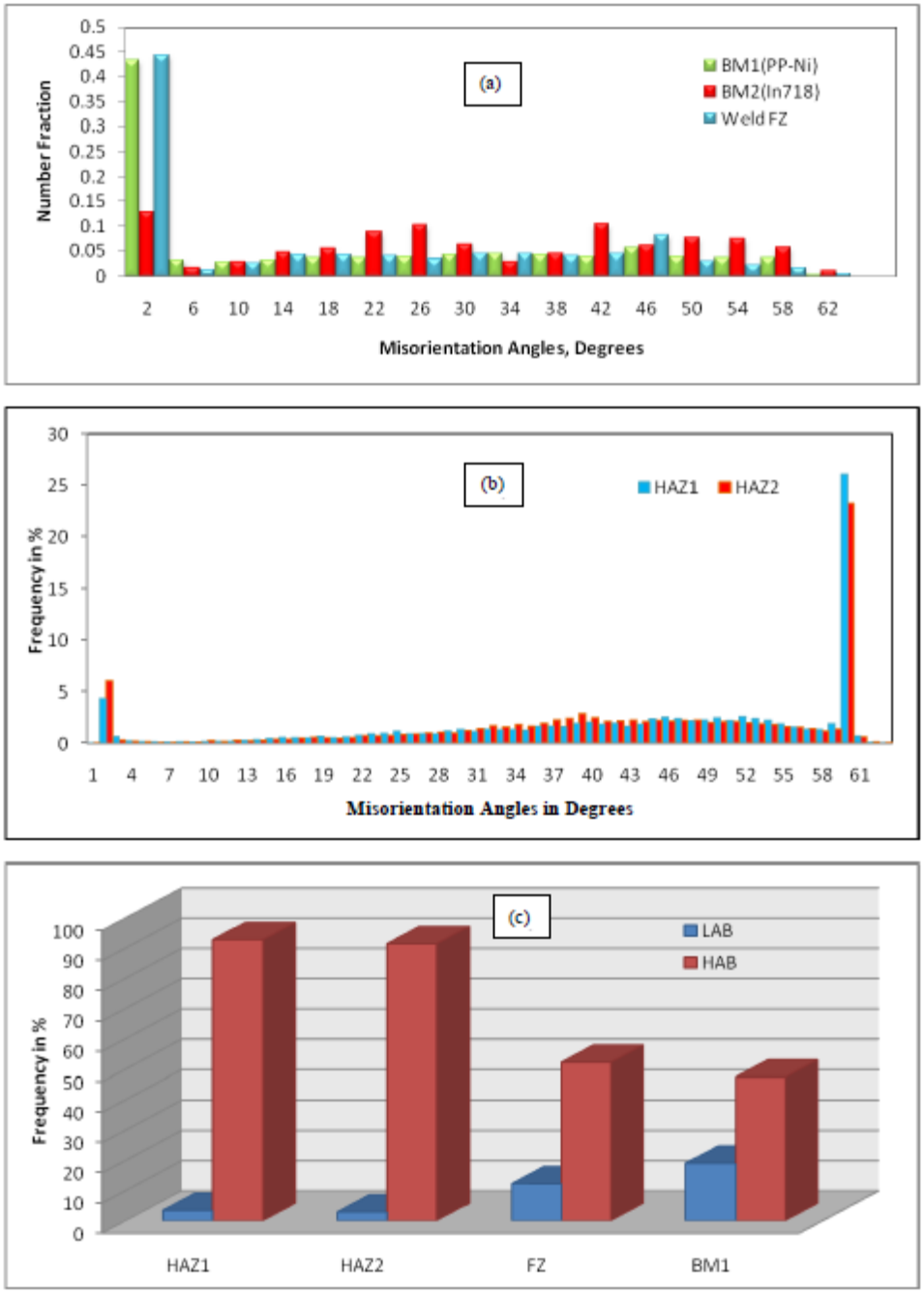

Figure 4 Misorientation distributions in (a) PP-Ni, IN718 and FZ and (b) CGHAZ (HAZ1) and FGHAZ (HAZ2). (c) HAB and LAB grain boundary misorientation data.

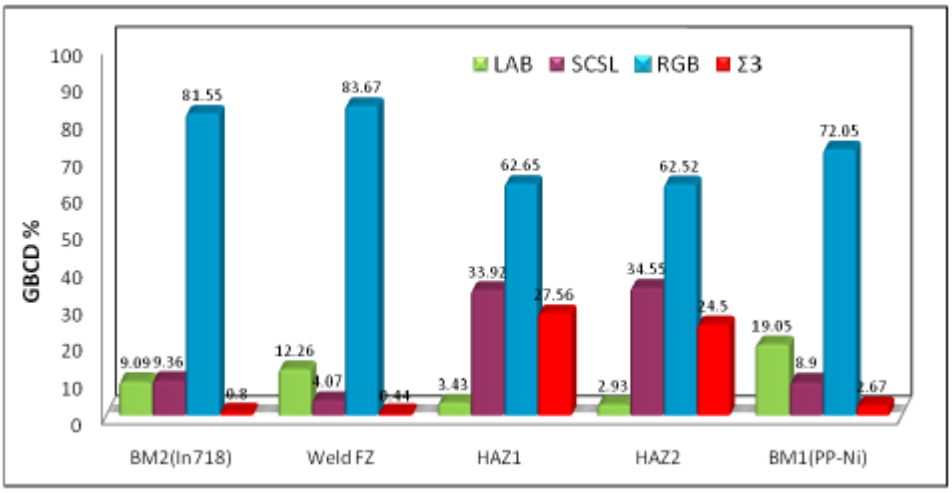

Figure 5 Calculated grain boundary characteristic distributions.

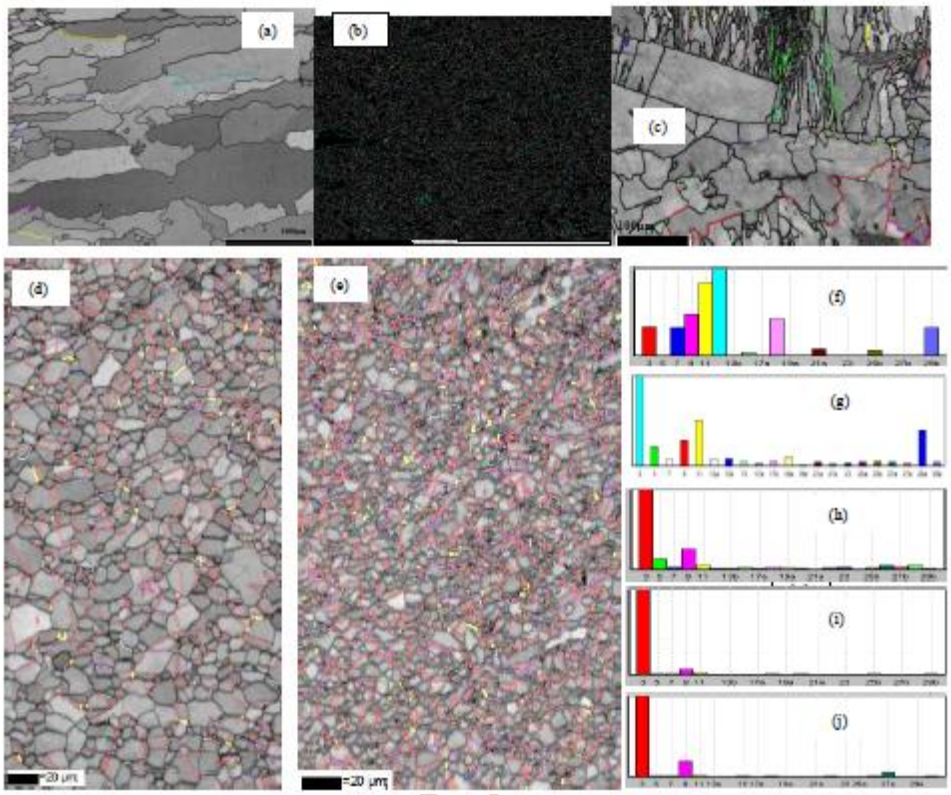

Figure 6 SCSL maps for (a) IN718, (b) PP-Ni, (c) Weld FZ, (d) CGHAZ and (e) FGHAZ. (f)-(j) show the respective statistical distributions. (Note: Readers are referred to the web version on this article for the interpretation of the reference to colour in the figure legend.)

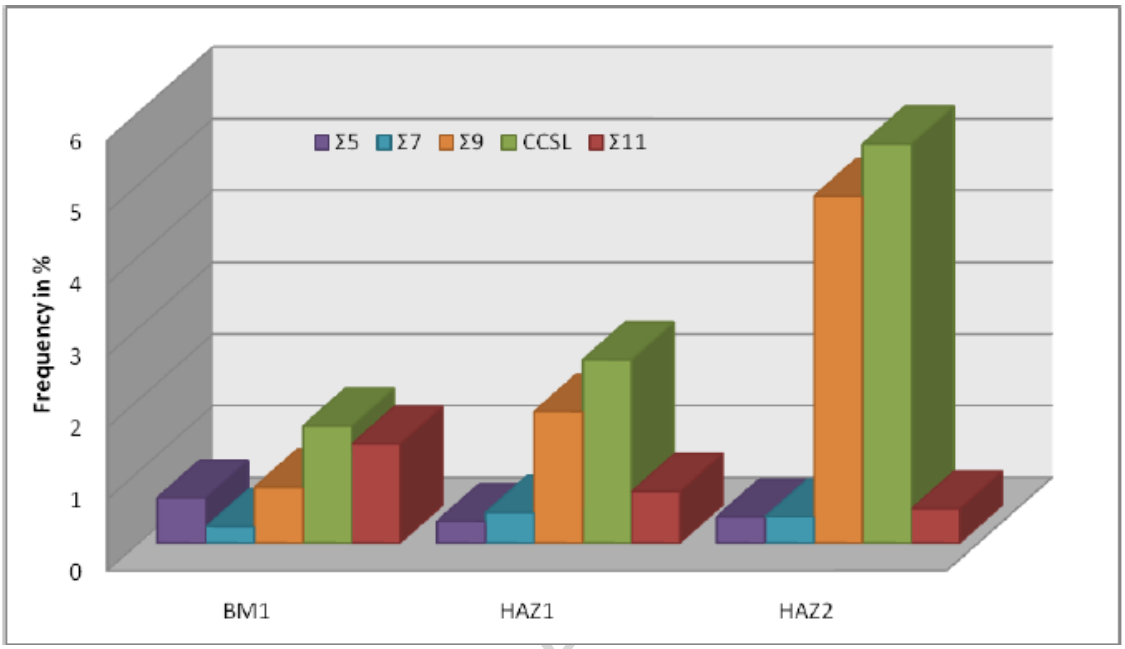

Figure 7 SCSL distributions in PP-Ni base metal (BM1), HAZ1 and HAZ2.

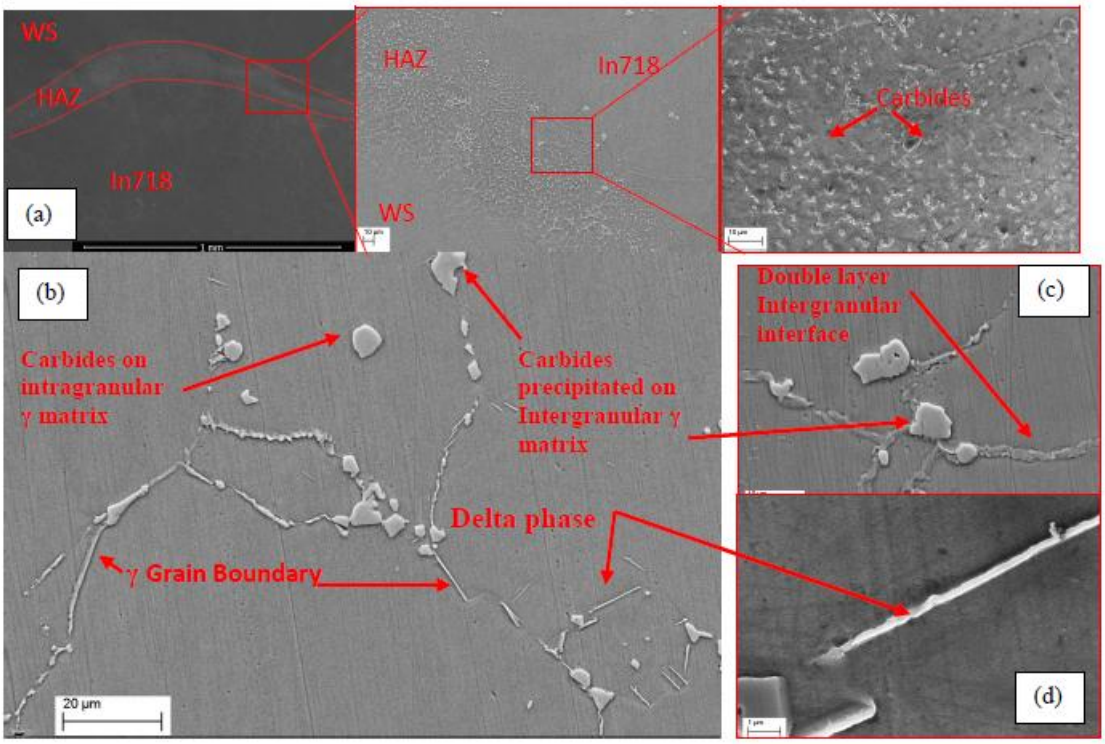

Figure8 SEM observations for (a) the HAZ on IN718 side of the dissimilar weld joint near the top of the weldment (yellow boxes in figure 1 (c)). (b) Secondary carbide phases (block shaped) and delta phase (needles/rods) on gamma (γ) grain boundaries on the IN718 side of the HAZ. (c) Carbide phase and microscale double layer grain boundary interface on γ grain boundaries. (d) Magnified view of needle shape delta phase on γ grain boundary. (Note: Readers are referred to the web version on this article for the interpretation of the reference to colour in the figure legend.)

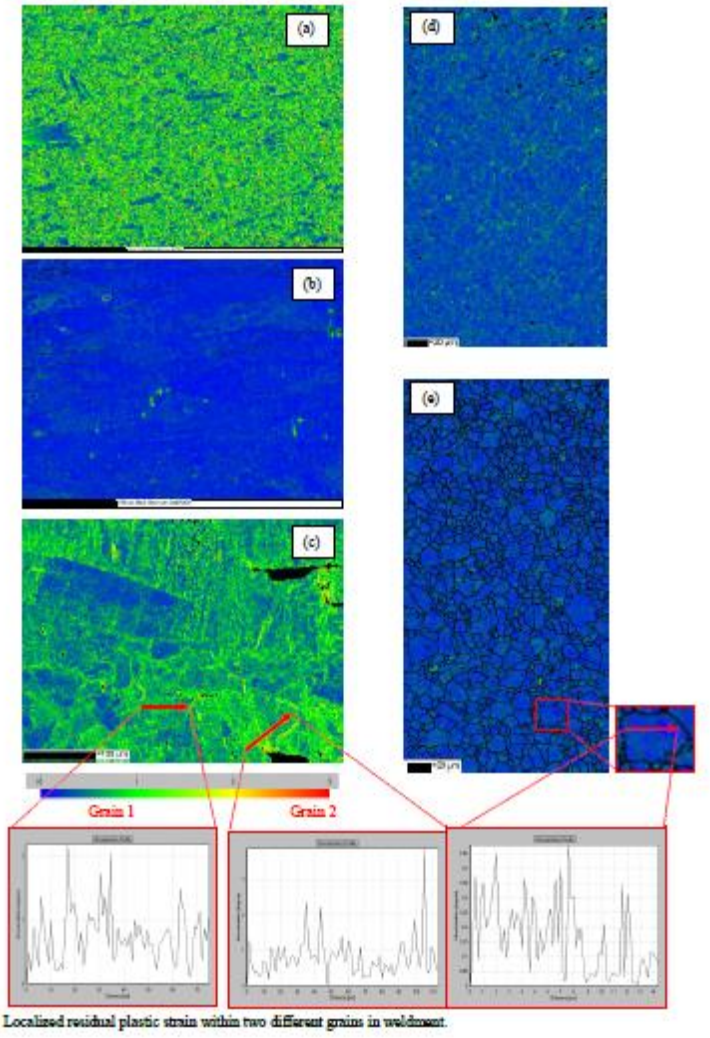

Figure 9 Map of local residual plastic strain concentrations in (a) PP-Ni, (b) IN718, (c) FZ, (d) HAZ2 and (e) HAZ1. Blue represents low local residual plastic strain concentration and red represents high residual plastic strain concentration. Note: Readers need to refer the web version of this article for interpretation of the references to legend colour in this figure.

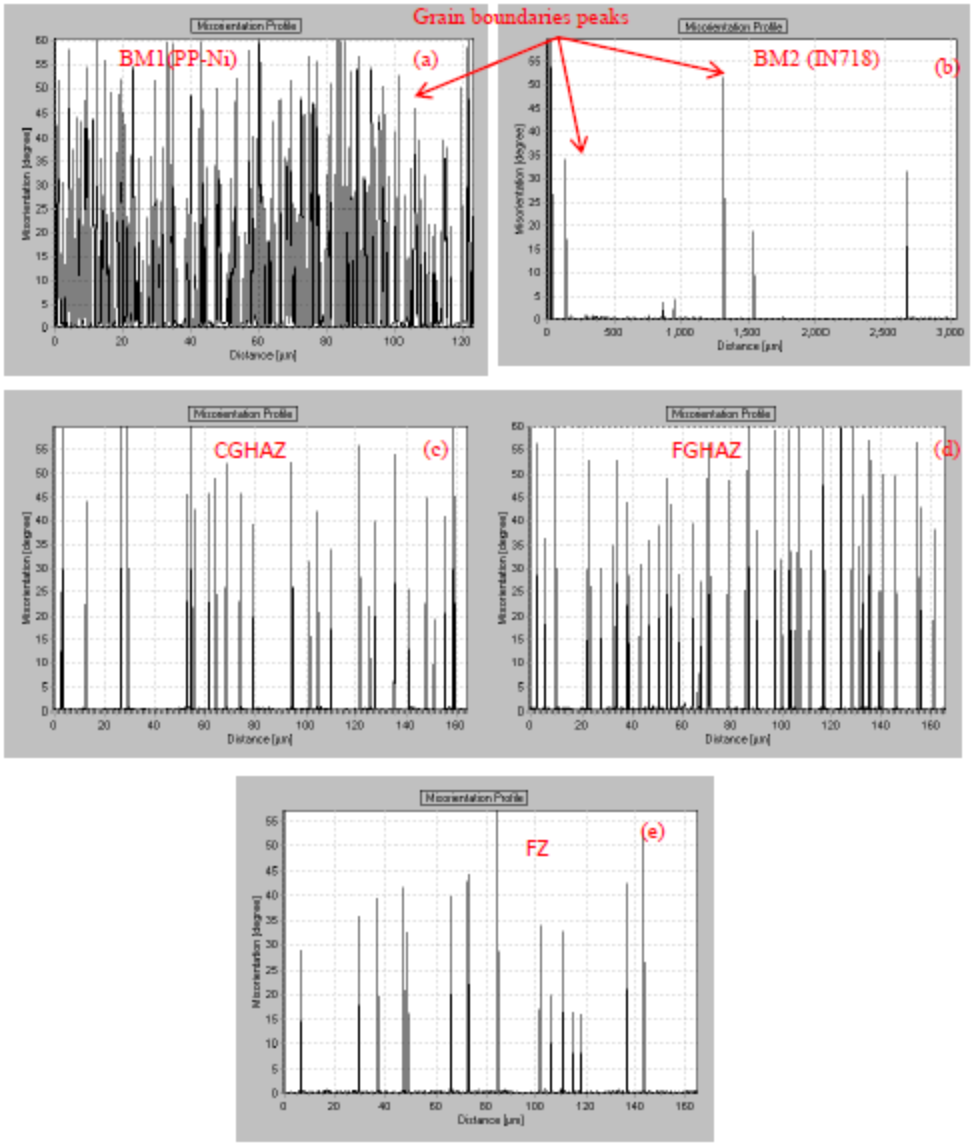

Figure 10 Calculated local misorientations plotted as a function of distance along TD on (a) PP-Ni, (b) IN718, (c) HAZ1, (d) HAZ2 and (e) FZ.

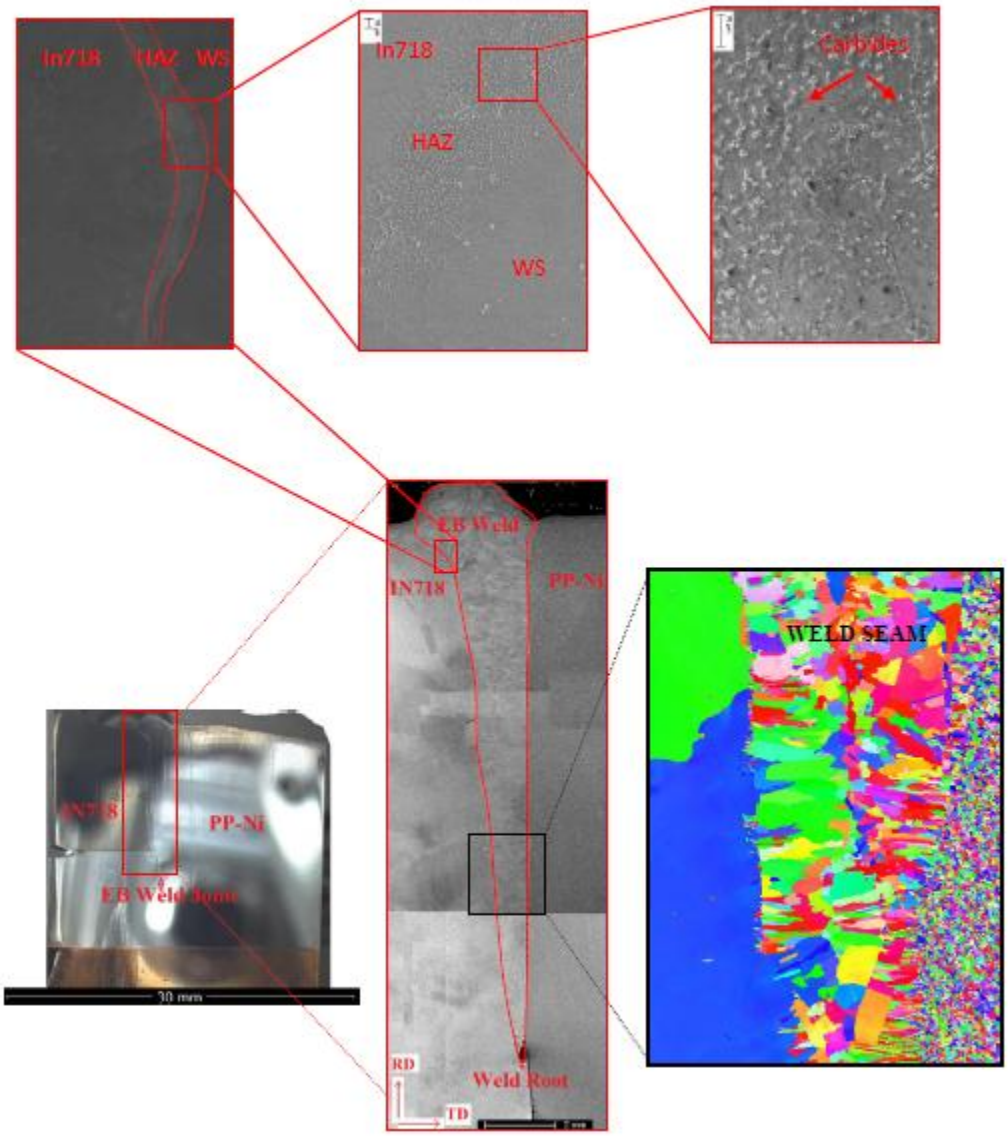

Graphical abstract

Highlights

- Microstructure evolution in dissimilar weld joint was investigated.
- Areas examined included the base metals, weld fusion zone and HAZs of weld joint.
- SEM/EBSD was employed to measure the residual plastic strain, crystal orientation.
- Grain boundary characteristic and grain structure distributions are also examined.
- The influence of microstructural features on hydrogen diffusion has been discussed.